Jestr

Journal of Engineering Science and Technology Review 9 (3) (2016) 176 - 186

Research Article

JOURNAL OF
Engineering Science and Technology Review

www.jestr.org

Mechatronic Rail Vehicle Design Based on the Passenger Comfort

Mortadha Graa[1], **MohamedNejlaoui**[1], **Ajmi Houidi**[2], **Zouhaier Affi**[1,*] and **Lotfi Romdhane**[1, 3]

[1]*Laboratoire de Génie Mécanique (LGM), Ecole Nationale d'Ingénieurs de Monastir, Université de Monastir, Rue Ibn El Jazzar - Monastir – 5000, Tunisie*
[2]*Laboratoire de Mécanique de Sousse (LMS), Institut Supérieur des Sciences Appliquées et de Technologie de Sousse, Université de Sousse, Sousse Ibn Khouldoun 4003, Tunisie*
[3]*College of Engineering, the American University of Sharjah, Sharjah, UAE*

Received 17 April 2016; Accepted 29 June 2016

Abstract

This paper deals with the mechatronic design of the rail vehicle (MRV) in order to improve the passenger comfort. The quarter rail vehicle system dynamic model is presented. The real characteristic of the actuator are discussed and its controller is designed. A mechatronic model that expresses the controlled tracking error as function of the vehicle dynamics and the actuator characteristics is developed. This model is used by the LQR approach to identify the MRV controller gains. The MRV comfort is evaluated in terms of the passenger displacement, acceleration and frequency as a response of a rail discontinuity and rail leveling defaults. The obtained results prove that the MRV improve significantly the passenger comfort.

Keywords: Mechatronic, actuator, rail vehicle, LQR, PID, comfort.

1 Introduction

Passenger comfort is one of the important criteria used to evaluate the performance of rail vehicles (RV). This comfort is highly affected by the vehicle speed and the rail imperfections. Improving the RV performance is the key to avoid high perturbations transmitted from the wheels to the passenger.

Several studies have been performed on RV as a pure mechanical system. Nejlaoui et al [1] optimized the structural design of a passive suspension in order to ensure simultaneously passenger safety and comfort. Abood et al [2] investigated the Railway carriage simulation model to study the influence of the vertical secondary suspension stiffness on ride comfort of a railway car body. Zhang et al [3] developed a finite elements optimization technique to find the best parameters of a passive suspension in order to improve the train riding comfort. Wang et al [4] proposed a multi-objective optimization strategy for the design of hydraulic dampers in the case of a vertical passive suspension in high-speed trains, in order to improve their ride comfort and stability.

In order to improve the RV performance, some researchers have considered the electro-mechanic design of the RV. They added an active suspension to the RV where a controlled actuator is embedded in the system [16]. Zhou et al [7] have developed an active lateral secondary suspension of an RV in order to attenuate the vehicle body lateral vibration. This active suspension is controlled by the use of skyhook dampers and modal control approach. Sezer et al [8] have controlled the vibration of the RV using a Fuzzy Logic Controller (FLC). To decrease the effect of road vibration problems, Eski et al [9] have controlled the vibration of the vehicle suspension by using a PID controller. Sun et al [17] have designed a dynamic feedback H_∞ controller for active seat suspension by considering limited frequency characteristics. The LQR method was also used in the design of active suspensions [5, 6]. The most drawback of the active suspension, as electro-mechanical approach, is that the mechanical system, the actuator and the controller are treated as separated subsystem.

Mechatronic design considers the close interaction of mechanics, actuators and control engineering in order to achieve a design with better performances. Important improvements of the rail vehicle performance could be achieved by using mechatronic approach [21]. More significantly, incorporation of the mechanical structure, the sensors, the controllers and actuators into the design process of vehicle, as a mechatronic approach, take more advantage in term of performance compared to the purely mechanical or electro mechanical design approach [24]. R Dumitrescu et al [22] have applied the mechatronic approach in order to support engineers from different disciplines to develop self-optimizing systems where the rail vehicle is considered as an example. T.X. Mei et al [23] have presented and discussed various mechatronic vehicle configurations based on the curving performance of the wheelset and ride quality of the vehicle.

This work deals with the mechatronic rail vehicle design based on the passenger comfort. A mechatronic model that expresses the controlled tracking error, describing the passenger comfort, as a function of the vehicle dynamics and the actuator characteristics simultaneously is developed. This model is used by the LQR approach to identify the MRV controller gains. This paper is organized as follows. In section 2, the vertical dynamic model of the RV is developed. In section 3, the dynamics of the used actuator is pre-

* E-mail address: nejlaouimohamed@gmail.com
ISSN: 1791-2377

sented. In section 4, the mechatronic RV (MRV) design is investigated. The results and comfort improvement discussed in section 5. Finally, concluding remarks are given in Section 6.

2 Dynamic Modeling of a Rail Vehicle

It is common to consider only the quarter of the RV model for the vertical dynamic studies of the RV system [6, 12]. The objective is to have a relatively simple model useful for the study of the dynamic behavior and even for the optimization of the RV structural parameters. In what follows, all the results are determined at the centers of mass of the different rigid bodies. Figure 1 illustrates an actuated quarter RV model with a passenger seat

The quarter model is made of a wheel, ½ bogie, ¼ car body and a passenger seat. The second suspension includes an actuator that generates a force $u(t)$ in parallel with its stiffness and dumper. This arrangement reduces the actuator size and dissipates the unwanted vibrations of the car body, in order to improve the comfort. The passive component provides the force supporting the car body mass in the vertical direction and ensures the reliability of the suspension system.

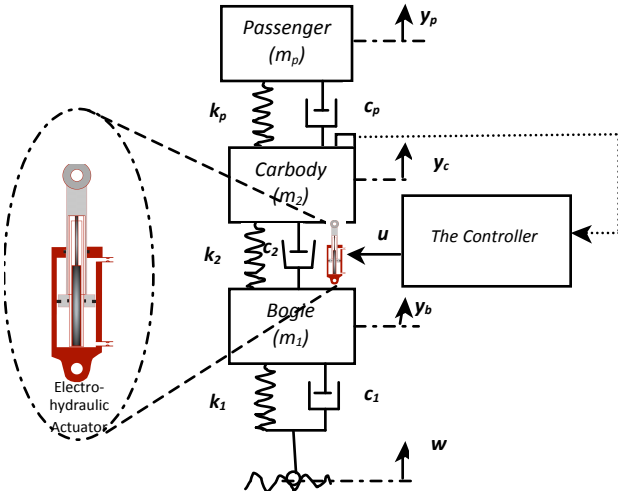

Fig. 1. An actuated quarter RV model.

Based on the Lagrange formulation, the quarter RV vertical motion can be given by the following equations:

$$\begin{cases} m_p\ddot{y}_p + k_p(y_p - y_c) + c_p(\dot{y}_p - \dot{y}_c) = 0 \\ m_2\ddot{y}_c - k_p(y_p - y_c) - c_p(\dot{y}_p - \dot{y}_c) - c_2(\dot{y}_c - \dot{y}_b) + k_2(y_c - y_b) = u \\ m_1\ddot{y}_b - k_2(y_c - y_b) + c_2(\dot{y}_c - \dot{y}_b) + k_1(y_b - w) - c_1(\dot{y}_b - \dot{w}) = -u \end{cases} \quad (1)$$

Where u is the actuator force

By adopting the following state space formulation vector:

$$\boldsymbol{X} = [x_1, x_2, x_3, x_4, x_5, x_6]^T = [y_p, \dot{y}_p, y_c, \dot{y}_c, y_b, \dot{y}_b]^T \quad (2)$$

The previous Eq. (1) can be written as:

$$\begin{cases} \dot{x}_1 = x_2 \\ \dot{x}_2 = \ddot{x}_1 = \ddot{y}_p = -\frac{1}{m_p}\left[k_p(x_1 - x_3) + c_p(x_2 - x_4)\right] \\ \dot{x}_3 = x_4 \\ \dot{x}_4 = \ddot{y}_c = -\frac{1}{m_2}\left[k_p(x_3 - x_1) + c_p(x_4 - x_2) + k_2(x_3 - x_5) + c_2(x_4 - x_6) - u\right] \\ \dot{x}_5 = x_6 \\ \dot{x}_6 = \ddot{x}_2 = -\frac{1}{m_1}\left[k_2(x_5 - x_3) + k_1(x_5 - w) + c_1(x_6 - \dot{w}) - c_2(x_4 - x_6) + u\right] \end{cases} \quad (3)$$

The matrix form of Equation (3) is as follows:

$$\begin{cases} \dot{\boldsymbol{X}} = \boldsymbol{A}\boldsymbol{X} + [\ \boldsymbol{B}\quad \boldsymbol{E}\quad \boldsymbol{F}\ ] \begin{bmatrix} u \\ w \\ \dot{w} \end{bmatrix} \\ \boldsymbol{Y} = \boldsymbol{C}\boldsymbol{X} + \boldsymbol{D} \begin{bmatrix} u \\ w \\ \dot{w} \end{bmatrix} \end{cases} \quad (4)$$

In Equation (4), $\boldsymbol{X}$ is the state vector for the 3-DOF suspension system and $\boldsymbol{Y}$ is the output vector, which includes the passenger displacement and acceleration. w is the disturbance signal caused by the irregularity of the railway track profile and $\dot{w}$ is its derivative. $\boldsymbol{A}$, $\boldsymbol{B}$, $\boldsymbol{C}$, $\boldsymbol{D}$, $\boldsymbol{E}$ and $\boldsymbol{F}$ are the coefficients matrices given by:

$$\boldsymbol{A} = \begin{bmatrix} 0 & 1 & 0 & 0 & 0 & 0 \\ -\frac{k_p}{m_p} & -\frac{c_p}{m_p} & \frac{k_p}{m_p} & \frac{c_p}{m_p} & 0 & 0 \\ 0 & 0 & 0 & 1 & 0 & 0 \\ \frac{k_p}{m_2} & \frac{c_p}{m_2} & -\frac{k_p}{m_2} - \frac{k_2}{m_2} & -\frac{(c_p + c_2)}{m_2} & \frac{k_2}{m_2} & \frac{c_2}{m_2} \\ 0 & 0 & 0 & 0 & 0 & 1 \\ 0 & 0 & \frac{k_2}{m_1} & \frac{c_2}{m_1} & -\frac{k_2}{m_1} - \frac{k_1}{m_1} & -\frac{c_1 + c_2}{m_1} \end{bmatrix}$$

$$\boldsymbol{B} = \begin{bmatrix} 0 & 0 & 0 & \frac{1}{m_2} & 0 & -\frac{1}{m_1} \end{bmatrix}^T;$$

$$\boldsymbol{C} = \begin{bmatrix} 1 & 0 & 0 & 0 & 0 & 0 \\ -\frac{k_p}{m_p} & -\frac{c_p}{m_p} & \frac{k_p}{m_p} & \frac{c_p}{m_p} & 0 & 0 \end{bmatrix};$$

$$\boldsymbol{D} = \begin{bmatrix} 0 & 0 & 0 \\ 0 & 0 & 1 \end{bmatrix};$$

$$\boldsymbol{E} = \begin{bmatrix} 0 & 0 & 0 & 0 & 0 & \frac{k_1}{m_1} \end{bmatrix}^T;$$

$$\boldsymbol{F} = \begin{bmatrix} 0 & 0 & 0 & 0 & 0 & \frac{c_1}{m_1} \end{bmatrix}^T;$$

The dynamic model with passive suspension can be obtained by canceling the actuator force u (t) in the previous model (eq.4).

3 Actuator

The selection of the actuator is made by taking into consideration the possible benefits such as the maintainability, the

reliability and the achievable control force. Hence, an electro-hydraulic actuator is used for this study [12, 18, 19]. The structure of an electro-hydraulic actuator is shown in Figure 2. A general description of the model of the actuator will be presented here.

The current *i* driving the spool is given as:

$$i = k_a v \tag{5}$$

where k_a is the gain of the servo-valve drive amplifier.

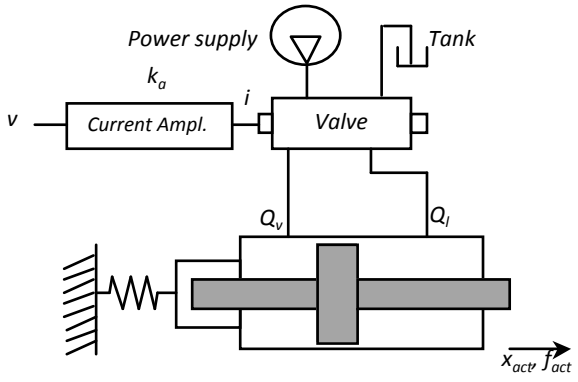

Fig. 2. Electro hydraulic actuator model.

The transfer function of the servo valve is generally of second order and can be expressed as:

$$H(s) = \frac{\omega^2}{s^2 + 2\zeta\omega s + \omega^2} \tag{6}$$

where ω is the servo valve frequency and ζ is the damping ratio.

The equation of the valve flow is:

$$Q_v = k_q H(s) i \tag{7}$$

The cross-port leakage flow Q_l is defined as:

$$Q_l = k_l \left[\frac{k_{oil}(x_a - x_{act})}{A_c} \right] \tag{8}$$

The required flow of the actuator is given by:

$$Q = A_c \dot{x}_a \tag{9}$$

The resultant actuator force can be expressed as:

$$f_{act} = k_{oil}(x_a - x_{act}) - B_{oil}\dot{x}_{act} \tag{10}$$

The maximum force that can be developed by the actuator is given by:

$$F_{\max} = \eta P_s A_c \tag{11}$$

Generally, the electro-hydraulic actuators are unstable [18, 19] .To solves this problem, in order to its integration in the MRV and considers the real characteristics of the actuator, the design of a controller for servo valve is necessary. For this goal, a lead-lag compensator is designed. Figure 3 shows the block diagram of the hydraulic actuator. The control force u(t) and the actuator extension velocity $\dot{x}_{act}$ are the system inputs, and the output is the actuator force f_{act} .

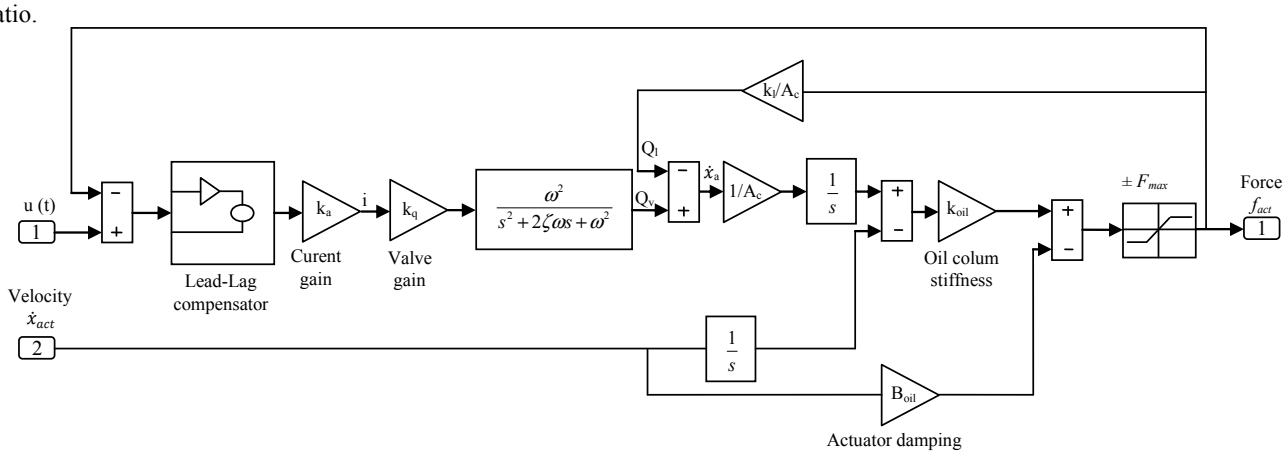

Fig. 3. Block diagram of a hydraulic actuator.

4 The MRV design

4.1 The MRV mechatronic model

For the MRV design, the dynamic RV model, the actuator characteristics and the controller are considered simultaneously. The controller is needed to identify the hydraulic force generated by the actuator to compensate the track disturbances. This force is generated by the hydraulic actuator to improve the MRV comfort. The track disturbance represents the car body motion relative to the bogie generated by the RV dynamic behavior. It is worth mentioning that these motions can be viewed as the output of the RV dynamics model as presented by Eq. (1). Figure 4 represents the mechatronic structure of the MRV system.

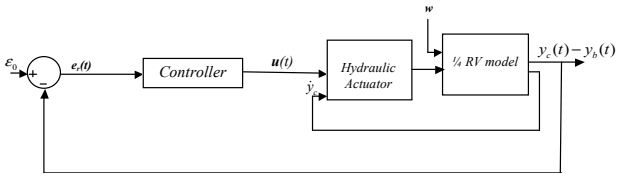

Fig. 4. Structure of the MRV.

ε_0 is the initial deflexion between the car body and the bogie

Since the actuator control the relative car body movement ($y_c(t)$) relative to the bogie ($y_b(t)$), we can write:

$$\begin{aligned} &m_2(\ddot{y}_c(t)-\ddot{y}_b(t))+c_2(\dot{y}_c(t)-\dot{y}_b(t)) \\ &+k_2(y_c(t)-y_b(t)-\varepsilon_0)=-u_c(t) \end{aligned} \quad (12)$$

The extension of the actuator from its original position is given by:

$$y_c(t)-y_b(t)-\varepsilon_0 = x_{act}(t)-x_a(t) \quad (13)$$

Using Eq.(8) and Eq.(13), the Eq.(12) can be written as follows:

$$u_c(t)=-\left[\frac{m_2 A_c}{k_l k_{oil}}\ddot{Q}_l(t)+\frac{c_2 A_c}{k_l k_{oil}}\dot{Q}_l(t)+\frac{k_2 A_c}{k_l k_{oil}}Q_l(t)\right] \quad (14)$$

The closed loop error of the MRV can be viewed as a change of the valve flow $Q_R(t)$ relative to its steady state situation $Q_l(t)$. In this case, we have:

$$Q_R(t)-Q_l(t)=e(t) \quad (15)$$

Initially, the valve flow $Q_R(t)=0$. Based on Eq. (15), we have:

$$-Q_l(t)=e(t) \quad (16)$$

In this case, Eq. (14) becomes,

$$\ddot{e}(t)+2\xi^0\omega^0\dot{e}(t)+(\omega^0)^2 e(t)=K' u_c(t) \quad (17)$$

Where:

$$K'=\frac{k_l k_{oil}}{m_2 A_c};\quad \omega^0=\sqrt{\frac{k_2}{m_2}};\quad \xi^0=\frac{c_2}{2m_2\omega^0} \quad (18)$$

If we consider the error, its integral and its derivative of the MRV as state variables presented by:

$$z_1(t)=\int e(t)dt\ ;\ z_2(t)=e(t)\ \ ;\ z_3(t)=\frac{de(t)}{dt} \quad (19)$$

The canonic representation of the Eq. (17), representing the state of the MRV can be expressed as:

$$\dot{\mathbf{Z}}=\mathbf{A'Z}+\mathbf{B'}u_c(t) \quad (20)$$

Where:

$$\boldsymbol{A'}=\begin{bmatrix}0 & 1 & 0\\ 0 & 0 & 1\\ 0 & -(\omega^0)^2 & -2\xi^0\omega^0\end{bmatrix};\quad \boldsymbol{B'}=\begin{bmatrix}0\\0\\K'\end{bmatrix};\boldsymbol{Z}=\begin{bmatrix}z_1(t)\\z_2(t)\\z_3(t)\end{bmatrix} \quad (21)$$

One can note that Eq. 20 represents the canonic form of the MRV mechatronic model. This model regroups simultaneously the tracking error, which will be controlled to improve the MRV passenger comfort, representing the output of RV dynamic model, the parameter of the second suspension and the actuator characteristics. The interesting mechatronic model can by useful for the design of different controllers types.

4.2 The MRV controller design

In this section, the PID controller will be tuned via the LQR approach based on the MRV mechatronic model. In fact, the more common controllers is the PID regulators. In fact, despite the identification complexity of the PID parameters for complex systems, this controller has the advantage of being easy to implement in common industrial processes. To solve the problem of gain identification, LQR approach, which leads to a good set-point tracking, is used. Therefore, the MRV can be viewed as shown in Figure 5.

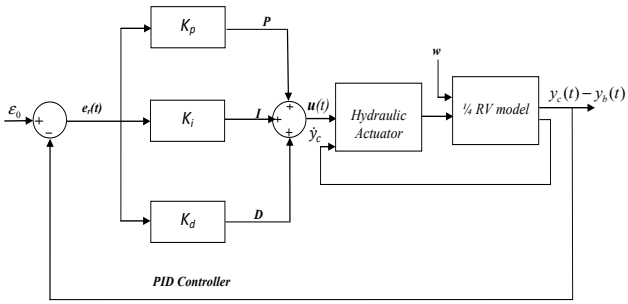

Fig. 5. PID controller of the MRV.

In order to tune the PID, through the LQR formulation, the following quadratic cost function, based on eq. 20, should be minimized:

$$J(\boldsymbol{Z}(t),u_c)=\int_0^\infty\left(\boldsymbol{Z}^{\boldsymbol{T}}(t)\boldsymbol{Q'}\boldsymbol{Z}(t)+u_c^T(t)\boldsymbol{R'}u_c^T(t)\right)dt \quad (22)$$

This cost function represents the control energy,

The weighting matrix $\boldsymbol{Q'}$ is diagonal positive definite and the weighting factor $\boldsymbol{R'}$ is a positive constant. The choice of the weighting matrix $\boldsymbol{Q'}$ and the constant $\boldsymbol{R'}$ is given by the Bryson's rule method [10] as:

$$\boldsymbol{Q'}=\frac{1}{\max\left(z_i^{\,2}\right)}\qquad \boldsymbol{R'}=\frac{1}{\max\left(u_c^{\,2}\right)} \quad (23)$$

The minimization of the cost function (Eq. (22)) gives the optimal control input as:

$$u_c(t)=-\boldsymbol{R'^{-1}}.\boldsymbol{B'^T}.\boldsymbol{P'}.\boldsymbol{Z}(t)=-\boldsymbol{F'}.\boldsymbol{Z}(t)=\begin{bmatrix}K_i & K_p & K_d\end{bmatrix}.\boldsymbol{Z}(t) \quad (24)$$

Where $\boldsymbol{P'}$ is the symmetric positive definite solution of the continuous Algebraic Riccatti equation (ARE) given by

$$\boldsymbol{P'}.\boldsymbol{A'}+\boldsymbol{A'^T}.\boldsymbol{P'}-\boldsymbol{P'B'R'^{-1}}.\boldsymbol{B'^T}.\boldsymbol{P'}+\boldsymbol{Q'}=\boldsymbol{0} \quad (25)$$

From Eq. (24), the corresponding state feedback gain matrix $\boldsymbol{F'}$ is given as follows:

$$\boldsymbol{F'} = \boldsymbol{R'^{-1}}.\boldsymbol{B'^{T}}.\boldsymbol{P'} = \begin{bmatrix} K_i & K_p & K_d \end{bmatrix} \quad (26)$$

Hence, the PID controller gains can be obtained.

5 Results and Dicussion

In this section, two rail disturbances will be considered i.e. the rail discontinuity and the rail leveling. The RV dynamic model used for the mechatronic system design will be validated by ADAMS. The naturals frequencies will be determined and the most sever one will be considered. A lead-Lag compensator, which grants the stability of actuator response, will be designed. The designed mechatronic rail vehicle performance in term of comfort will be presented and discussed.

5.1 Rail design parameters

The first default type is a step function applied at the center of the wheel. It presents a local discontinuity default H at the rail head (figure 6). This default is defined as:

$$w(t) = \begin{cases} 0 & if\ 0 \le t \le 1 \\ H & Otherwise \end{cases} \quad (27)$$

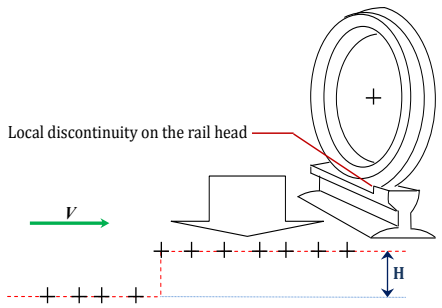

Fig. 6. Rail discontinuity default.

The second rail default is a longitudinal one. It is given in figure 7 [11]:

$$w(t) = \begin{cases} -\frac{H}{2}\left[1-\cos\left(2\pi\frac{V}{D}t\right)\right] & if\ 0 \le t \le \frac{D}{V} \\ 0 & Otherwise \end{cases} \quad (28)$$

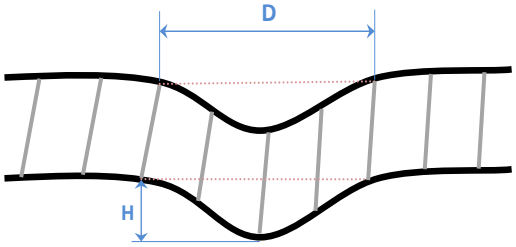

Fig. 7. Rail leveling default.

V is the vehicle longitudinal velocity. We consider V=130km/h=36.11m/s, H=0.03m and $D = \frac{V}{N_1} = 50\,m$.

The parameters used for these simulations are given in Table 1.

Table 1. The RV design parameters [**6**].

Parameters	*Values*
m_p	*80 kg*
m_2	*24740 kg*
m_1	*3200 kg*
k_p	*18000 N/m*
k_2	*600000 N/m*
k_1	*4360000 N/m*
c_p	*600 Ns/m*
c_2	*40000 Ns/m*

5.2 The dynamic RV model validation

To solve the obtained differential equations, describing the RV dynamic model, we have used the Runge-Kutta method [20]. The dynamic model of the RV is solved using MATLAB and validated by ADAMS. Figure 8 shows the evolution of the passenger center of mass where the input of the system w is a step function which is more severe than the leveling default.

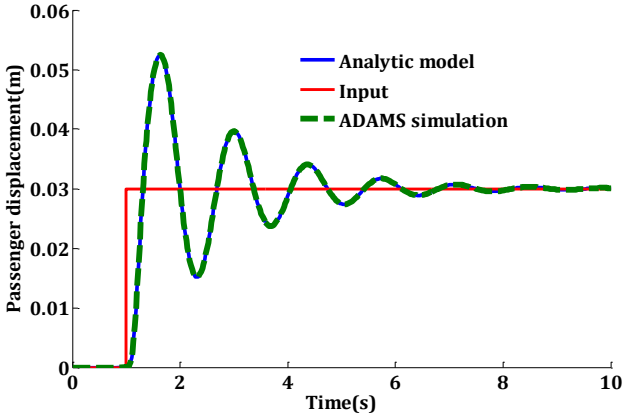

Fig. 8. Validation of the analytical model by ADAMS.

A frequency analysis is conducted in order to find the natural frequencies of the system. Figure 8 shows the Bode diagrams of the RV response. One can note that the system has three natural frequencies, 0.73Hz, 2.53Hz and 5.8Hz whose magnitude amplifications are, respectively, 12.7 dB, -8.42dB and -31.2dB (Figure 9). The most severe is N1= 0.73Hz. In what follows, this critical frequency will be used for the different simulations in order to show the performances of the MRV system compared to the RV one.

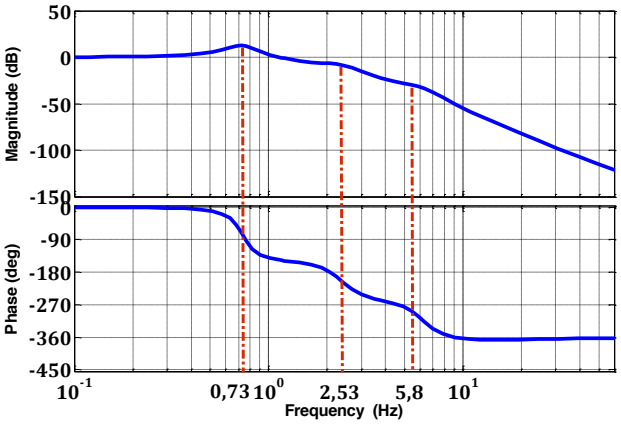

Fig. 9. Bode diagram of the quarter RV system.

5.3 Stability of the actuator

The electro-hydraulic actuator parameters adopted for this study are listed in Table 2.

Table 2. Actuator parameters [19]

Parameter	Value
k_a	2.5×10^{-3} A/V
k_q	1.24×10^{-3} $m^3/s/A$
k_l	$1.48\times10^{-14} m^5 s^{-1}/Nm$
A_c	$3.372\times10^{-4} m2$
k_{oil}	8.19×10^{6} N/m
ζ	0.4
ω	628.32 rad/s
η	0.67
P_s	206842800 Pa
F_{max}	46.73 KN
v_{max}	0.082m/s
B_{oil}	471.24 N/m

The Nichols chart from the voltage input to the force output, is given in Figure 10. One can note that the uncompensated actuator system is unstable and cannot be integrated directly in the MRV system. To solve this problem, a Lead Lag compensator is designed for the servo valve. The controller is tuned to give an acceptable gain and phase margins.

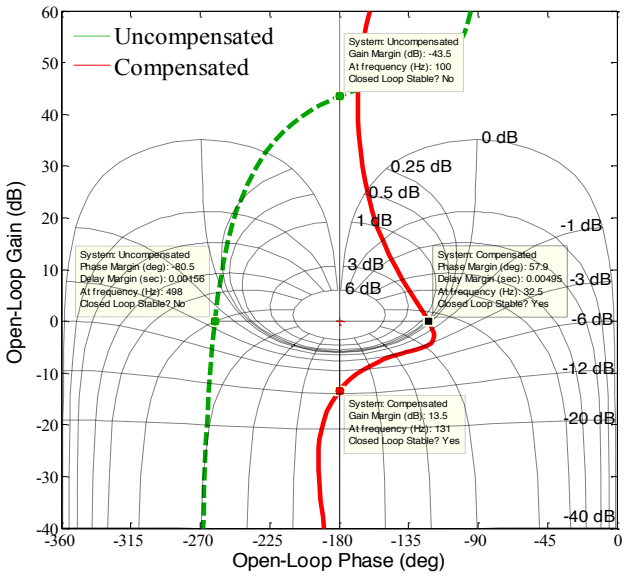

Fig. 10. Nichols chart for the RV actuator dynamic.

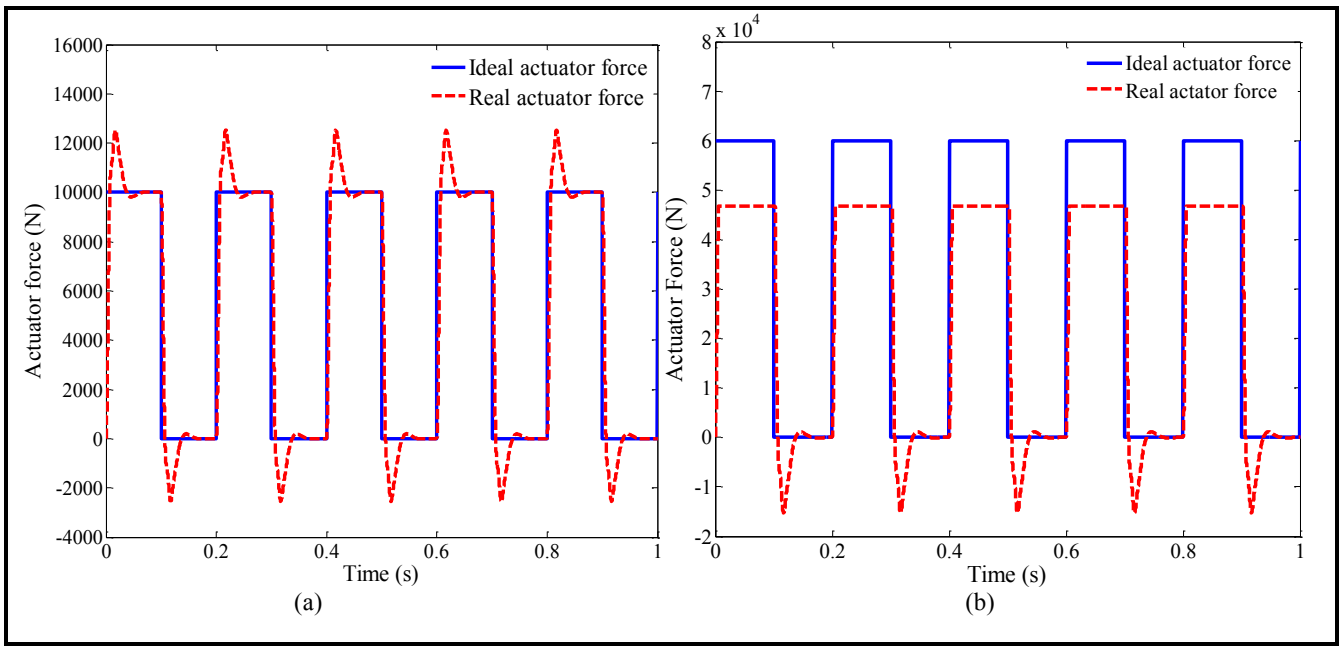

Fig. 11. Force following of the actuator.

The Lead-lag compensator is designed in order to give the actuator a gain margin of 13.5 dB, and a phase margin of 57.9° (Figure 10). In this case, the transfer function of the lead-lag compensator is given by:

$$H(s)=\frac{\left(1.0933\times10^{-3}s+1\right)}{\left(3.3311\times10^{-7}s+1\right)}\frac{\left(0.0089s+1\right)}{\left(4.115s+1\right)}V/N \qquad (29)$$

To show the effectiveness of the designed Lead Lag compensator, we will show the electro-hydraulic actuator response to a square-wave power demand of 10 KN and 60 kN at 10Hz. Figure (11 .(a))and Figure (11.(b)) show that the response of the actuator is stable and give an adequate response to a square-wave power excitation. Figure (11.(b)) confirms, in particular, that the actuator saturation force is considered.

5.4 Stability of the hybrid controller

By considering the state space given by the mechatronic model (Eq. 20) and the LQR approach the PID gains, given by Eq. 26, are presented in Table 3:

Table 3. The PID gains

		K_p	K_d	K_i
Active gains	***PID-LQR***	3690.52	538.39	1804.34

According to the Nichols chart presented by Figure 12, the phase margin of MRV system is 30° at frequency of 3.2Hz. Hence, the MRV response is stable.

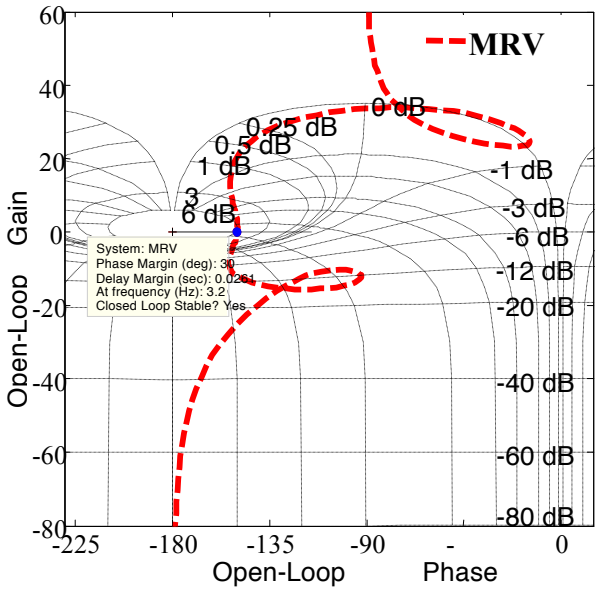

Fig. 12. Nichols chart for MRV.

5.5 Evaluation of the comfort

In this section, the passenger comfort is evaluated using two criteria. The first one is the passenger vertical displacement and the second one is the passenger vertical acceleration. The performances of the comfort are evaluated in term of rise time (T_R), maximum peak to peak (MPTP) and settling time (T_S).

The improvement of RV performance by adopting the MRV approach is defined by:

$$\text{Imp}\ (\%) = \left|\frac{A-B}{A}\right| 100 \tag{30}$$

Where:

A: value obtained with a classical RV.
B: value obtained with the MRV.

5.5.1 Passenger comfort evaluated in term of displacement

Figures13 and 14 present the vertical passenger displacement, in case of a rail leveling and rail discontinuity defaults. It can be observed that, in the case of the MRV, the reduction of the passenger's vertical displacement peak is approximately 96% for the case of rail leveling default, and 40% for the rail discontinuity case, compared to RV system.

Moreover, the MRV has the best result in terms of T_R, T_S and MPTP for both cases of rail defaults. In fact, in the case of rail leveling default, the improvement of MPTP is more than 97%, T_R is reduced from 1.36 to 1.2 sec and T_S is reduced from 5.13 sec to 1.2sec in the case of the RV (Table 4).

Table 4. Results of comfort with MRV for longitudinal leveling default (D=50m).

D=50m	T_R(s)	Imp T_R (%)	T_S(s)	ImpT_S (%)	MPTP (m)	Imp MPTP (%)
RV	*1.36*	-	*5.13*	-	*0.07*	-
MRV	*1.25*	*8.08*	*1.20*	*76.6*	*2 e-3*	*97.14*

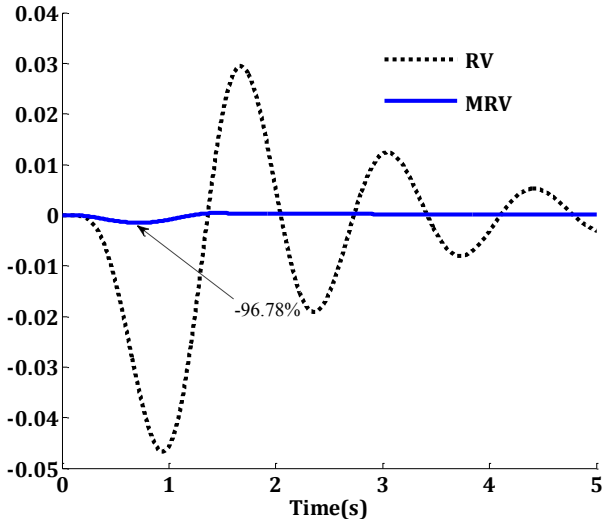

Fig. 13. Passenger displacement for rail leveling default.

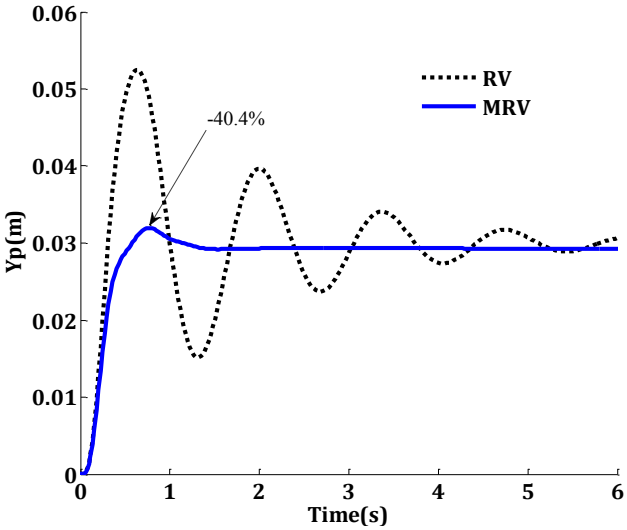

Fig. 14. Passenger displacement for rail discontinuity default.

5.5.2 Passenger comfort in terms of vibration and frequecy

The used criterion to evaluate the passenger comfort in term of vibration and frequency is described in the international standard ISO 2631-1[13].This standard uses the Root Mean Square (RMS) value of the passenger vertical acceleration, which is defined as:

$$RMS = \left[\frac{1}{T}\int_0^T [a(t)]^2\ dt\right]^{0.5} \tag{31}$$

where $a(t)$ is a weighted vertical acceleration expressed in m/s², and T is the time exposure duration, in sec.

$a(t)$ is obtained by filtering the passenger vertical acceleration signal $\ddot{y}_p(t)$ through the filter W_k given in Figure 15 and defined in the 1997 ISO 2631-1 standard [13].

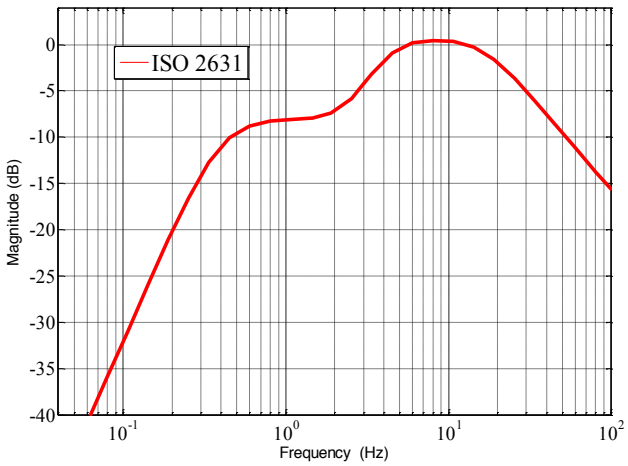

Fig. 15. Frequency weighting curve W_k (ISO 2631) [13]

The evaluation of the comfort was carried out by comparing the value of *RMS* to the comfort level in the ISO 2631 standard given in the Table 5.

Table 5. The comfort level rated by ISO 2631[13].

RMS Values (m/s^2)	Description
$RMS < 0.2$	Very Comfortable
$0.2 \le RMS < 0.3$	Comfortable
$0.3 \le RMS < 0.4$	Average
$RMS \ge 0.4$	Less Comfortable

Figures 16-17 show the evolution of the vertical passenger acceleration with RV and MRV in both cases of rail defaults.

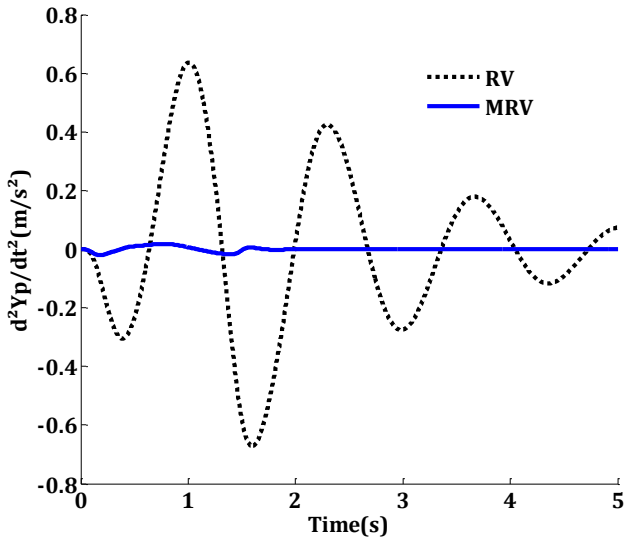

Fig. 16. Passenger acceleration for rail leveling default.

From Table 6, it can be observed that the passenger peak acceleration, for local discontinuity default, is reduced by 68% in case of MRV compared to RV one. The settling time is also significantly reduced from 4.7 sec to 0.8 sec (82%).

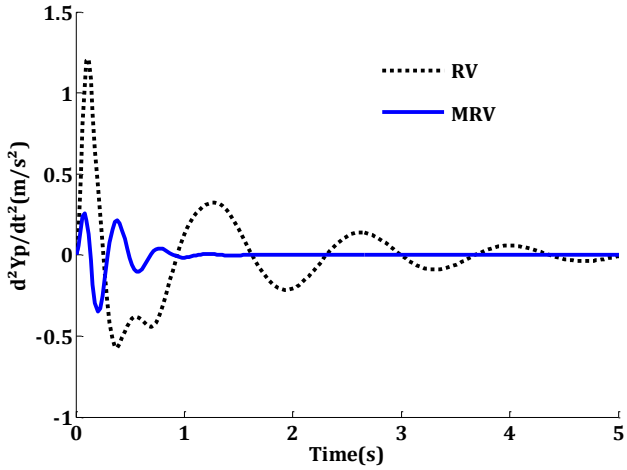

Fig. 17. Passenger acceleration for rail discontinuity default.

Table 6. Passenger acceleration for rail discontinuity default.

	Settling time(s)	ImpSettling time (%)	Peak (m/s²)	Imp Peak (%)
RV	*4.7*	-	*1.12*	-
MRV	*0.8*	*82.97*	*0.36*	*67.85*

From Table 7, it can also be noted that the passenger peak acceleration for rail leveling default is reduced by 97%, when using MRV. Moreover, the settling time is significantly reduced from 5.2 sec to 1.5 sec (70%).

Table 7. Passenger acceleration for rail leveling default (D=50m).

D=50m	Settling time (s)	Imp Settling time (%)	Peak (m/s²)	Imp Peak (%)
RV	*5.2*	-	*0.63*	-
MRV	*1.51*	*70.96*	*0.01*	*97.30*

From Table 8, one can note that the MRV presents a lower RMS acceleration than the RV one. The passenger comfort level is improved by about 95%.

We can also note from Table 8 a high level of the MRV comfort compared to the RV one. Figure 18 gives the actuator force that generates this comfort level.

Table 8. Results of comfort quantification for longitudinal leveling default (D=50m).

D=50m	*RMS (m/s^2)*	*Imp (%)*	*Rms Real actuator force (kN)*	*Rms Ideal actuator force (kN)*
RV	*1.6*	-	-	-
MRV	*0.03*	*95.12*	*4.62*	*3.67*

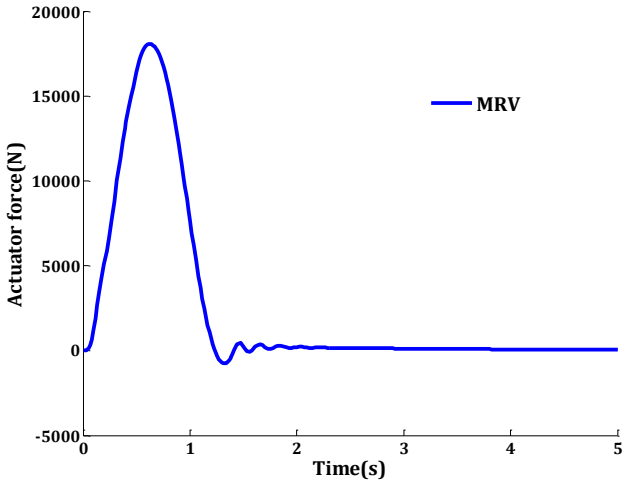

Fig. 18. Actuator force for rail leveling default (D=50m).

Figure 19 and Figure 20 show the evolution in the value of the passenger comfort (RMS) as function as, respectively, of the length of the rail longitudinal leveling default (D) and the height of the local discontinuity (H).

The MRV keeps a low RMS value compared to the RV system. According to Figure 18 and Figure 19, the MRV keeps the passenger in a very comfortable level (RMS<0.2) for all values of, respectively, D and H.

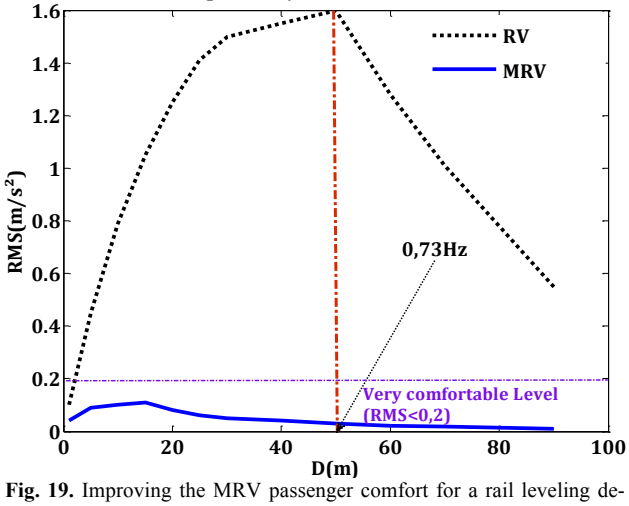

Fig. 19. Improving the MRV passenger comfort for a rail leveling default.

This result is proved in the frequency domain (Figure 21 and Table 9).The MRV magnitude improvement is, respectively, 311%, 156% and 36% in natural frequency, respectively, first, second and third.

Table 7. Quantification of improvement MRV in frequency domain.

Natural Frequency	N_1	N_2	N_3
Peak RV(dB)	*12.68*	*-8.74*	*-31.18*
Peak MRV(dB)	*-26.87*	*-22.44*	*-42.68*

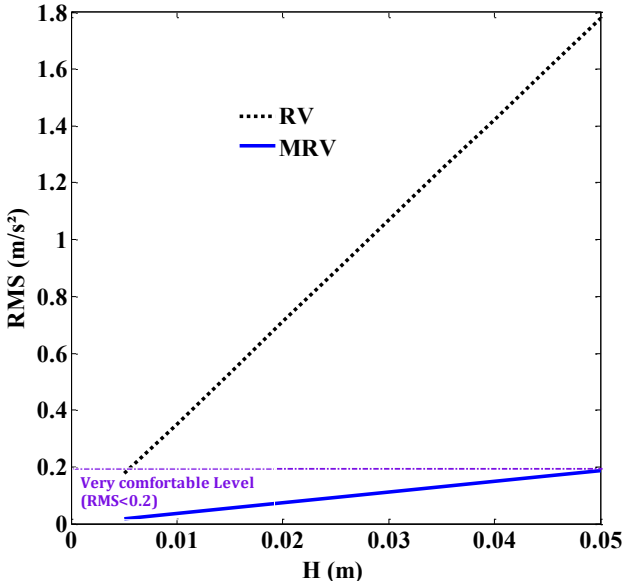

Fig. 20. The MRV passenger comfort for a rail discontinuity.

According to the ISO2631 the human body is more sensitive to vibrations between 4Hz and 8Hz in the vertical direction [6, 15], which corresponds to the third natural frequency (N_3=5.8Hz).In this range of frequency (Figure 21), the MRV improve significantly the magnitude. Which explain the improvement of the weighted RMS comfort (Eq. (30)).

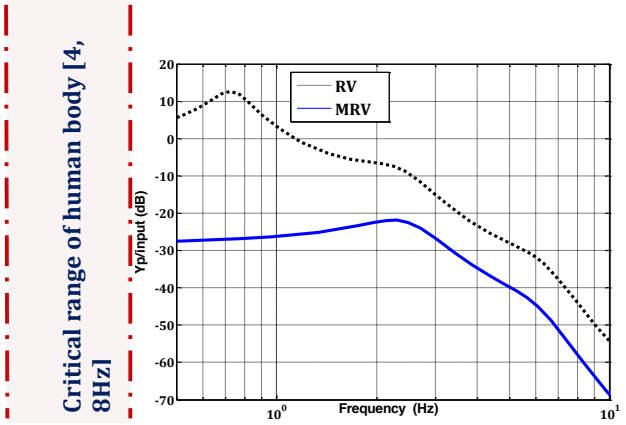

Fig. 21. Rail vehicle passenger responses in frequency domain.

6 Conclusion

In this work, we have presented a mechatronic design of the rail vehicle. The analytical vertical dynamic model of the quarter rail vehicle with a passenger seat is presented and validated by the ADAMS software. The real characteristic of the actuator are discussed and its lead lag compensator is designed. A mechatronic model that express the controlled tracking error as function of the vehicle dynamics and the actuator characteristics simultaneously is developed. Based on this model, the LQR approach is used to identify the PID gain for the MRV in order to improve the passenger comfort in terms of displacement, vibration, and frequency. The obtained results showed that the passenger's comfort is significantly improved. Moreover, the MRV passenger can have a very comfortable level in both cases of the considered rail imperfections.

References

1. M. Nejlaoui, A. Houidi, Z. Affi, L. Romdhane. Multiobjective robust design optimization of rail vehicle moving in short radius curved tracks based on the safety and comfort criteria. Simulation Modeling Practice and Theory 2013; 30:21–34.
2. K. H. A. Abood and R. A. Khan. The Railway carriage simulation model to study the influence of vertical secondary suspension stiffness on ride comfort of railway carboy. Journal of Mechanical Engineering Science 2011; 225:1349-1359.
3. Y.W. Zhang, Y. Zhao, Y.H. Zhang, J.H. Lin, and X.W. He. Riding comfort optimization of railway trains based on pseudo-excitation method and symplectic method. Journal of Sound and Vibration 2013; 332: 5255–5270.
4. W.L.Wang, X. J.Yang,G. X. Xu, and Y. Huang. Multi-objective design optimization of the complete valve system in an adjustable linear hydraulic damper. Journal of Mechanical Engineering Science 2011; 225:679-699.
5. Pratt I. Active Suspension Applied to Railway Trains. PhD Thesis, Department of Electronic and Electrical Engineering, Loughborough University, 2002.
6. Vincent. J. Etude du concept de suspensions actives-Applications aux voitures ferroviaires. PhD Thesis, INSA de Lyon, Fr, 1999.
7. R. Zhou, A. Zolotas and R. Goodall. 9 DOF railway vehicle modeling and control for the integrated tilting bolster with active lateral secondary suspension. IEEE, UKACC International Conference on Systems Technology Control 2010 ; 465 :1-6.
8. S. Sezer and A. E. Atalay. Dynamic modeling and fuzzy logic control of vibrations of a railway vehicle for different track irregularities. Simulation Modeling Practice and Theory 2011; 19:1873–1894.
9. I. Eski and S. Yıldırım. Vibration control of vehicle active suspension system using a new robust neural network control system. Simulation Modeling Practice and Theory, 2009; 17: 778–793.
10. R. S. Sanchez-Pena and M. Sznaier. Robust Systems: Theory and Applications. Adaptive and Learning Systems for Signal Processing Communications, and Control. John Wiley & Sons, Inc., New York, 1998.
11. K. Sasaki, S. Kamoshita, and M. Enomoto. A Design and Bench Test of Multi-Modal Active Suspension of Railway Vehicle. IECON'94, 20th International Conference on Industrial Electronics, Control and Instrumentation, 1994; 3: 2011–2016.
12. E. Foo and R.M. Goodall. Active Suspension Control of Flexible-Bodied Railway Vehicles Using Electro-Hydraulic and Electro-Magnetic Actuators. Control Engineering Practice, 2000; 8: 507–518.
13. ISO 2631: 2001. Mechanical Vibration and Shock-Evaluation of Human Exposure to Whole-Body Vibration. Part 4: Guidelines for the Evaluation of the Effects of Vibration and Rotational Motion on Passenger and Crew Comfort in Fixed Guide way Transport Systems.
14. Y. G. Kim, H.B. Kwon, S.W. Kim, C-K Kim and T.W Kim. Correlation of ride comfort evaluation methods for railway vehicles. Proceedings of the Institution of Mechanical Engineers. Part F: Journal of Rail and Rapid Transit 2003, 217.
15. CEN, EN 12299. Railway Applications- Ride comfort for passengers-Measurement and Evaluation, Brussels, April 2009.
16. Jonasson M, Roos F. Design and evaluation of an active electromechanical wheel suspension system. Mechatronics 2008; 18: 218-230.
17. Sun W, Li Jinfu, Zhao Y, Gao Huijun. Vibration control for active seat suspension systems via dynamic output feedback with limited frequency characteristic. Mechatronic 2011; 21:250-260.
18. Foo E, Goodall R. Active suspension control of flexible-bodied railway vehicles using electro-hydraulic and electro-magnetic actuators. Control Engineering Practice 8 (2000) 507-518.
19. Hazlina, Md Yusof. Technologies and control strategies for active railway suspension actuators. PhD Thesis, Loughborough University, 2012.
20. Halpern D, Wilson HB and Turcotte LH. Advanced mathematics and mechanics applications using MATLAB. 3rd ed. Boca Raton: Chapman & Hall/ CRC, 2003.
21. S Iwnicki Future trends in railway engineering Proc. IMechE Vol. 223 Part C: J. Mechanical Engineering Science.
22. R Dumitrescu1 et al Towards the design of cognitive functions in self-optimizing systems exemplified by a hybrid energy storage system Proc. IMechE Vol. 225 Part I: J. Systems and Control Engineering.
23. T.X. Mei Mechatronic solutions for high-speed railway vehicles Control Engineering Practice 10 (2002) 1023–1028.
24. R.M. Goodall and W. Kortüm Mechatronic developments for railway vehicles of the future Control Engineering Practice 10 (2002) 887–898.

Nomenclature

m_p	Passenger mass
m_1	Bogie mass
m_2	Car body mass
k_p	Stiffness of the passenger seat
k_1	Stiffness of the primary suspension
k_2	Stiffness of the secondary suspension
c_p	Damping coefficient of the passenger seat
c_1	Damping coefficient of the primary suspension
c_2	Damping coefficient of the secondary suspesion
w	Track rail irregularity input
K_i	Integrator coefficient of the PID controller
K_d	Derivative coefficient of the PID controller
K_p	Proportional coefficient of the PID controller
u	Desired control force
$y_b, \dot{y}_b, \ddot{y}_b$	Bogie displacement, speed and acceleration respectively
$y_c, \dot{y}_c, \ddot{y}_c$	Car body displacement, speed and acceleration respectively
$y_p, \dot{y}_p, \ddot{y}_p$	Passenger displacement, speed and acceleration respectively
k_a	Amplifier gain
k_q	Valve gain
k_l	Leakage gain
B_{oil}	Oil column damping
A_c	Cross sectional area cylinder
k_{oil}	Oil column stiffness
ζ	Damping of the servo valve
ω	Servo valve frequency
η	Efficiency of the actuator
P_s	Supply pressure
F_{max}	Maximum force
v_{max}	Ideal actuator velocity
i	Current driving spool
v	Servo valve voltage
Q_v	valve flow
RMS	Root Mean Square
RV	Rail vehicle
MRV	Mechatronic rail vehicle
N, N_2, N_3	First, second and third natural frequency of quarter RV respectively
T_R	Rise Time
T_S	Settling Time
x_a	Original position actuator
$x_{act}, \dot{x}_{act}$	actuator extension displacement and velocity respectively
H	Hauteur of longitudinal leveling or local discontinuity default
f_{act}	Actuator force
Q_l	Cross-port leakage
V	RV longitudinal velocity
D	Length of longitudinal leveling